08,09

Near-infrared Emission in $Na_5Y(WO_4)_4 : Nd^{3+}$

© A. Pusdekar[1], N.S. Ugemuge[1], R.A. Nafdey[2], S.V. Moharil[3]

[1] Department of Physics, Anand Niketan College,
Anandwan, Warora, 442907 India
[2] Department of Physics, Shri Ramdeobaba College of Engineering and Management,
Nagpur, 440013 India
[3] Department of Physics, RTM Nagpur University,
Nagpur, 440033 India

E-mail: pusdekarashvini2407@gmail.com

Received September 21, 2023
Revised September 21, 2023
Accepted September 25, 2023

Luminescence in $Na_5Y(WO_4)_4 : Nd^{3+}$ is investigated for the first time. The emission is in the near-infrared region. The well-known $^4F_{3/2} \rightarrow {}^4I_{9/2}$ transition leads to most intense line at 1069 nm. The excitation and emission spectra are interpreted using the energy level diagram of Nd^{3+}. The excitation spectrum is made up of a large number of sharp lines attributable to various $f-f$ transitions. A weak band at 360 nm in the excitation spectrum is assigned to the host. Notwithstanding large Y−Y distances, the luminescence is quenched at concentrations exceeding 2 mol.%. The critical distance for energy transfer among Nd^{3+} ions is found to be 32.85 Å.

Keywords: luminescence, phosphor, tungstate, Nd^{3+}.

DOI: 10.61011/PSS.2023.11.57329.208

1. Introduction

In the system $Na_2O-Y_2O_3-WO_3$, two compounds, $NaY(WO_4)_2$ and $Na_5Y(WO_4)_4$, are well known. Trunov et al. carried out pioneering investigations on synthesis and crystal structures of these compounds [1]. Of these, $NaY(WO_4)_2$ has been studied much more frequently. Hosts of this type involving tungstates of lanthanides and alkali/alkaline earth metals are well-known for their suitability to yield luminescent materials. Especially, solid state lasers based on such compositions are well-recognized. Low concentration quenching, host sensitization, emission well-separated from the excitation, long-lived excited states are some of the peculiarities of lanthanide luminescence in these hosts [2]. Though $Na_5Y(WO_4)_4$ has been known for nearly eighty years [3], luminescence in this host has been investigated only occasionally [4]. In $NaY(WO_4)_2$, Na and Y are randomly distributed and thus there is cation disorder. No such disorder exists for $Na_5Y(WO_4)_4$ [5]. Moreover, Y−Y distances are of the order 6.39 Å and well-isolated by virtue of intervening O−W−O links. As a consequence of this, concentration quenching related to energy transfer among RE ions at Y substitutional sites is minimum. In fact Qin et al. found no concentration quenching for Tb and Eu compounds [6].

Near-infrared (NIR) emission in $Na_5Y(WO_4)_4$ is not yet studied. Such emission can be important for various applications [7] like laser, telecommunication [8], bioimaging [9], photodynamic therapy, etc. Nd^{3+} ion is known to be a good activator for NIR emission. Nd^{3+} ion has been extensively used in the laser crystals. We chose Nd^{3+} as an activator to obtain NIR emission in $Na_5Y(WO_4)_4$ host. Preparation and luminescence of this phosphor are described in the following.

2. Experimental

Various $Na_5Y(WO_4)_4 : Nd^{3+}$ compositions were obtained using solid-state reaction. Na_2CO_3 (A.R., 99.5%), Y_2O_3 (A.R.), $Na_2WO_4 \cdot 2H_2O$ (A.R.), WO_3 (A.R.), Nd_2O_3 (99.99%) ingredients were used. These ingredients mixed in desired proportions were heated at 873 K for 12 hours. The typical chemical reaction for the synthesis of pure host material is given as follows:

$$\frac{1}{2}Na_2CO_3 + \frac{1}{2}Y_2O_3 + 2WO_3 + 2Na_2WO_4 \cdot 2H_2O \rightarrow Na_5Y(WO_4)_4 + \frac{1}{2}CO_2.$$

Formation of the desired compound was confirmed by studying X-ray diffraction (XRD) patterns. Philips XPERT-PRO diffractometer was used for this purpose. Photoluminescence (PL) characteristics in NIR region were measured on Photon Technology International QM-51 NIR spectrophotometer. Hitachi F-7000 spectrofluorometer was used to record reflectance spectra ($BaSO_4$ as an internal standard).

Scanning electron microscopy, energy dispersive spectroscopy (EDS), and elemental mapping were obtained on JEOL Model JSM 6380A scanning electron microscope.

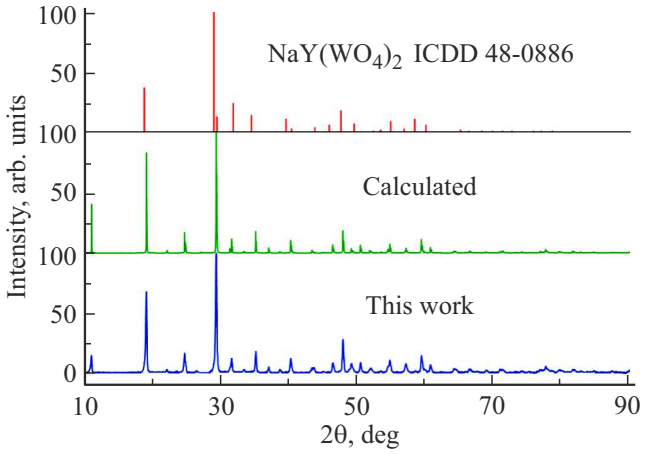

Figure 1. XRD pattern for $Na_5Y(WO_4)_4$. The experimentally obtained pattern is compared with the calculated. A good match is seen. To confirm phase purity, comparison was also made with XRD pattern of $NaY(WO_4)_2$. Absence of split line near 28.92° indicates that there is no formation of $NaY(WO_4)_2$.

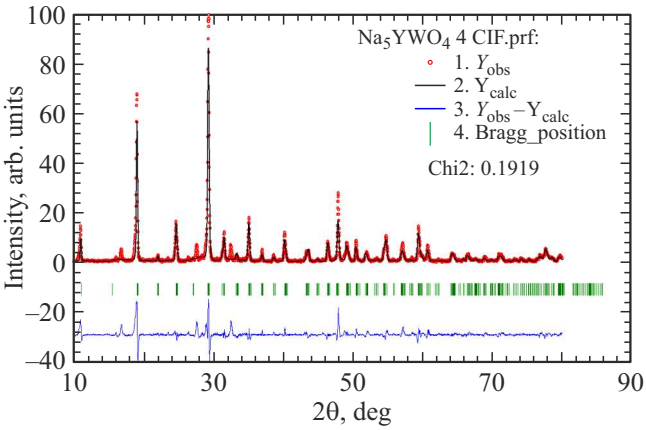

Figure 2. Rietveld refinement of XRD pattern for $Na_5Y(WO_4)_4$ using FullProf software.

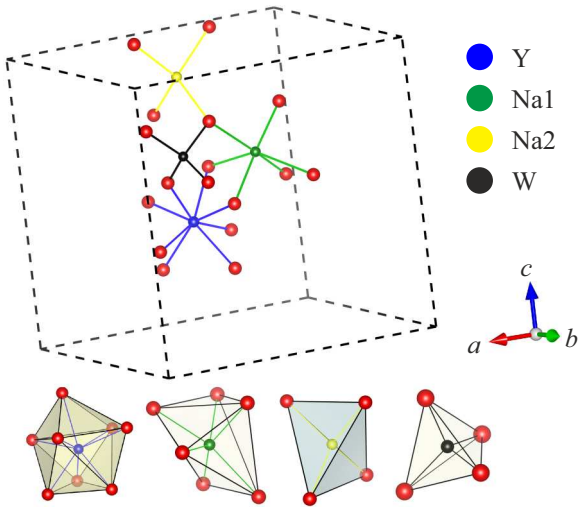

Figure 3. Crystal structure of $Na_5Y(WO_4)_4$. Coordination polyhedra for various cations are shown.

3. Results and discussions

Fig. 1 shows results of powder diffraction measurements. Distinct sharp lines were obtained. The experimentally obtained pattern is compared with the calculated one. An excellent match is seen. For comparison, standard data (ICDD 48-0886) corresponding to $NaY(WO_4)_2$ is also shown. The characteristic feature of $NaY(WO_4)_2$ is a split line around 28.92°. We do not observe such feature in the observed XRD pattern. Phase-pure $Na_5Y(WO_4)_4$ is thus formed. For $Na_5Y(WO_4)_4$ the system is tetragonal and crystallizes in $I4_1/a$ space group. There are four formula units in the cell.

Results of Rietveld refinement obtained using FullProf suite are shown in Fig. 2. The data converged to ($a = 11.414$ Å, $c = 11.35$ Å, $V = 1485.841$ Å^3. Goodness of fit can be judged by the parameter $\chi^2 = 0.1919$. Atomic coordinates are listed in Table 1.

The unit cell comprises of WO_4 tetrahedra (Fig. 3). Oxygen atoms can be distinguished on the basis of symmetry into four types O_1, O_2, O_3, and O_4. There are two types of Na sites with coordination 6 and 4. Coordination polyhedral for six coordinated Na_1 at Wyckoff site 4*b*. For four coordinated Na_2 the polyhedral are distorted tetrahedra [4]. Yttrium is 8-coordinated. WO_4 and YO_8 are connected via corners.

Fig. 4 shows results of EDS analysis and elemental mapping.

Relative percentages of constituent elements are shown in Table 2 and compared with those obtained from the

Table 1. Atomic coordinates for $Na_5Y(WO_4)_4$

Atom	Type	*X*	*Y*	*Z*	Occupancy
Na_1	Na	0.38073	0.03349	0.14698	1.00000
Na_2	Na	0.00000	0.25000	0.62500	0.25000
Y_1	Y	0.00000	0.25000	0.12500	0.25000
W_1	W	0.17954	0.15932	0.38568	1.00000
O_1	O	0.13338	0.10309	0.53046	1.00000
O_2	O	0.07376	0.15378	0.21742	1.00000
O_3	O	0.24435	0.48616	0.22448	1.00000
O_4	O	0.12870	0.28200	0.54612	1.00000

Table 2. Elemental analysis

Ser. No.	Element	At.% by formula	At.% observed
1	W	15.38	15.82
2	O	61.5	61.93
3	Na	19.23	18.44
4	Y	3.84	3.81
TOTAL		100	100

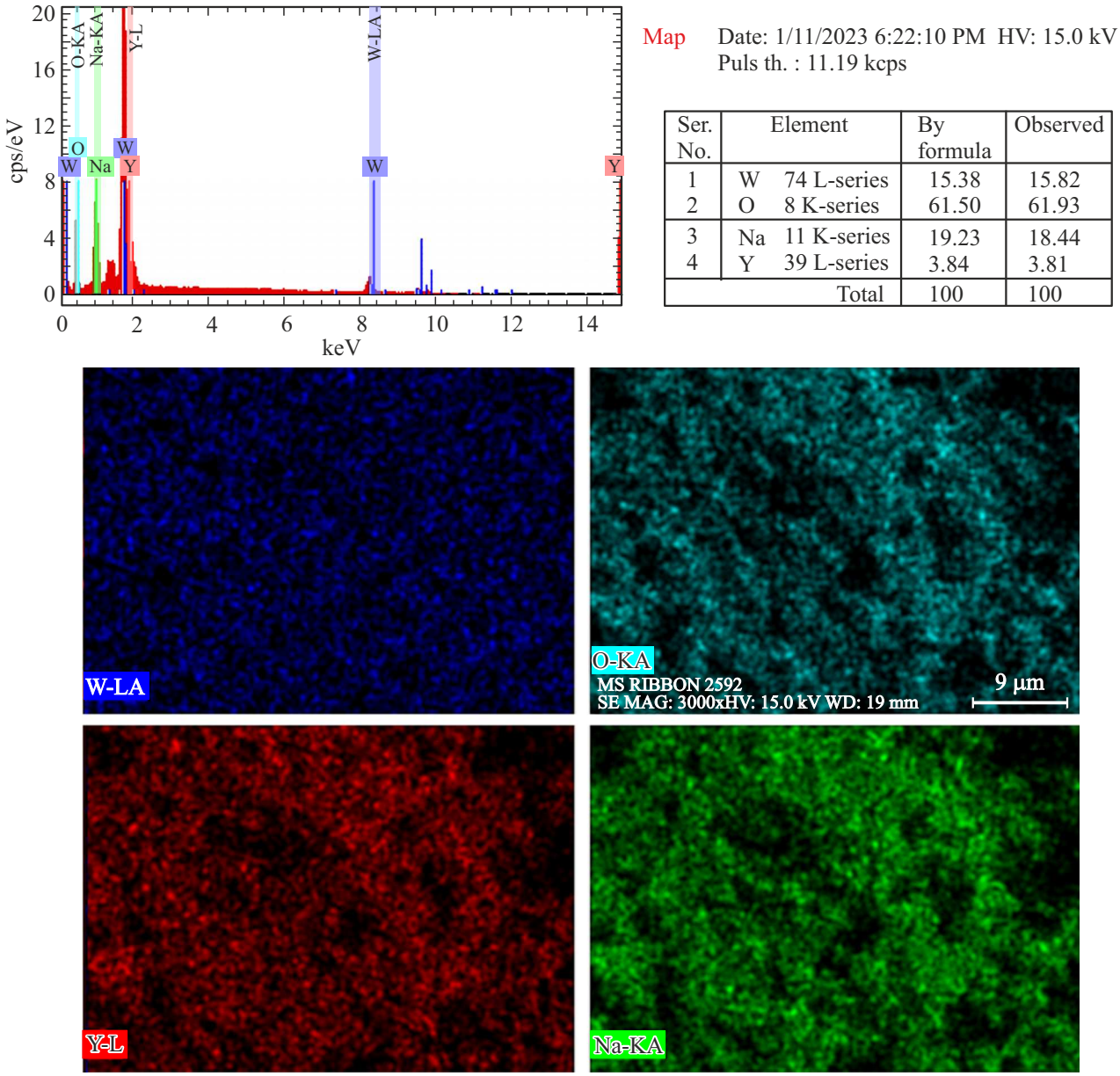

Ser. No.	Element	By formula	Observed
1	W 74 L-series	15.38	15.82
2	O 8 K-series	61.50	61.93
3	Na 11 K-series	19.23	18.44
4	Y 39 L-series	3.84	3.81
	Total	100	100

Figure 4. Results of EDS analysis and elemental mapping of $Na_5Y(WO_4)_4$.

formula $Na_5Y(WO_4)_4$. These two are in close agreement. Elemental mapping shows that these elements are uniformly distributed. All these results show that phase-pure $Na_5Y(WO_4)_4$ is formed.

Fig. 5 shows electron micrograph. Irregular particles of the size $5-30\,\mu$m can be seen.

Reflectance spectra were recorded for samples. Results for $Na_5Y(WO_4)_4$ are plotted in Fig. 6.

Kubelka–Munk functions are also plotted which are more closely related to absorption. Reflectance starts increasing from about 300 nm and reaches maximum at about 600 nm. Below 300 nm there is sharp drop in reflectance due to host absorption. These results are consistent with the earlier observations of Hammer et al. [4].

Fig. 7 shows the results of PL measurements for Nd^{3+}-doped sample.

588 nm excitation was used. The most intense emission is around 1069 nm. It has components at 1067 and 1083 nm. Weaker emission is observed around 880 nm. The two emissions are attributable to the transitions $^4F_{3/2} \rightarrow {}^4I_J$, $J = {}^4I_{9/2}$ and $^4I_{11/2}$, respectively. There is also another weak emission around 1350 nm owing to $^4F_{5/2} \rightarrow {}^4I_{13/2}$ transition, which is not shown in Fig. 7. All lines are considerably split. The splitting is due to the crystal field. Inset shows the emission intensity as a function of Nd concentration. Peak height of the 1069 nm emission line is used to plot this graph. Maximum intensity is observed for 2 mol.% Nd. The concentration dependence data enables estimation of the critical distance for energy transfer among

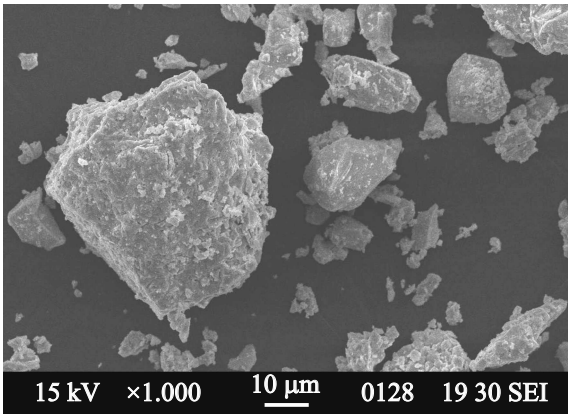

Figure 5. Electron micrograph of $Na_5Y(WO_4)_4$.

Nd^{3+} ions. The following formula [10] is used for this:

$$R_c = 2\left(\frac{3V}{4\pi x_c N}\right)^{1/3}.$$

Here, x_c is critical concentration (.02), N is number of Y sites in the unit cell (4), and V is volume of the unit cell (1485.841 Å^3). With these numbers, R_c is evaluated as 32.85 Å. The critical distance is thus quite large compared to 5 Å that is characteristic of $d-d$ interaction. Hence, it may be deduced that the quenching takes place through multipolar interactions.

Fig. 8 shows the corresponding excitation spectra. Sharp lines attributable to the $f-f$ transitions of Nd^{3+} make up the excitation spectra. These are tabulated in Table 3.

Apart from these intense $f-f$ excitation lines, there is a weak band at about 360 nm which could be due to tungstate group.

The emission and excitation spectra can be understood on the basis of the energy-level diagram for Nd^{3+} (Fig. 9).

Thus, Nd^{3+} ion reaches various excited states by absorbing light of wavelengths mentioned in Table 3. It then relaxes to the state $^2F_{5/2}$ by phonon creation. Transitions from this state to ^4I_J states lead to NIR emission.

Table 3. Various excitation lines for 1069 nm emission in $Na_5Y(WO_4)_4:Nd^{3+}$

Ser. No.	Transition	Position, nm
1	$^4I_{9/2} \rightarrow {}^2K_{11/2}$	477, 483
2	$^4I_{9/2} \rightarrow {}^4G_{7/2}, {}^2K_{13/2}$	519, 530
3	$^4I_{9/2} \rightarrow {}^4G_{5/2}, {}^2H_{11/2}$	579, 588, 596
4	$^4I_{9/2} \rightarrow {}^4F_{9/2}$	691
5	$^4I_{9/2} \rightarrow {}^4F_{7/2}, {}^4S_{3/2}$	744, 753
6	$^4I_{9/2} \rightarrow {}^4F_{5/2}$	806, 824
7	$^4I_{9/2} \rightarrow {}^4F_{3/2}$	885

Thus, intense NIR emission around 1069 nm which can be pumped using various wavelengths throughout the visible and NIR region is observed in $Na_5Y(WO_4)_4:Nd^{3+}$.

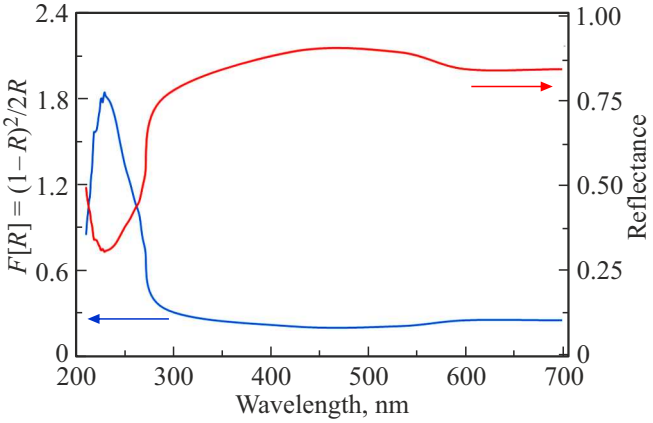

Figure 6. Reflectance spectra of $Na_5Y(WO_4)_4$. Kubelka–Munk functions $F[R] = (1-R)^2/2R$ are also plotted (left-hand-side ordinate) to get the idea about absorption.

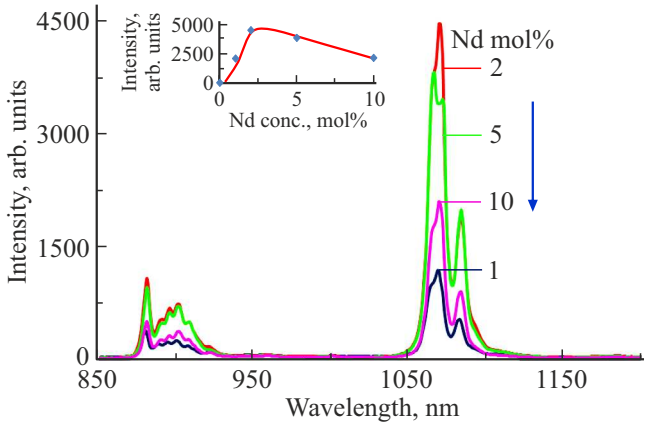

Figure 7. PL emission spectra for $Na_5Y(WO_4)_4:Nd^{3+}$. Emission was obtained with 588 nm excitation. Inset shows concentration dependence of the intensity. Peak height of the 1069 nm emission line is plotted as a function of concentration. Inset shows concentration dependence of the intensity.

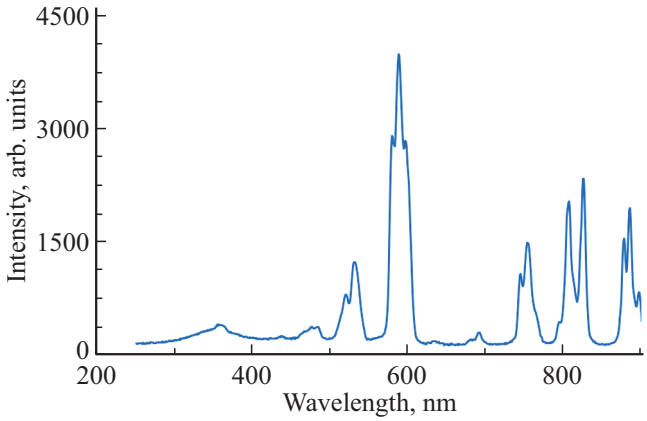

Figure 8. Excitation spectra for $Na_5Y(WO_4)_4:Nd^{3+}$. Excitation was monitored for 1069 nm emission.

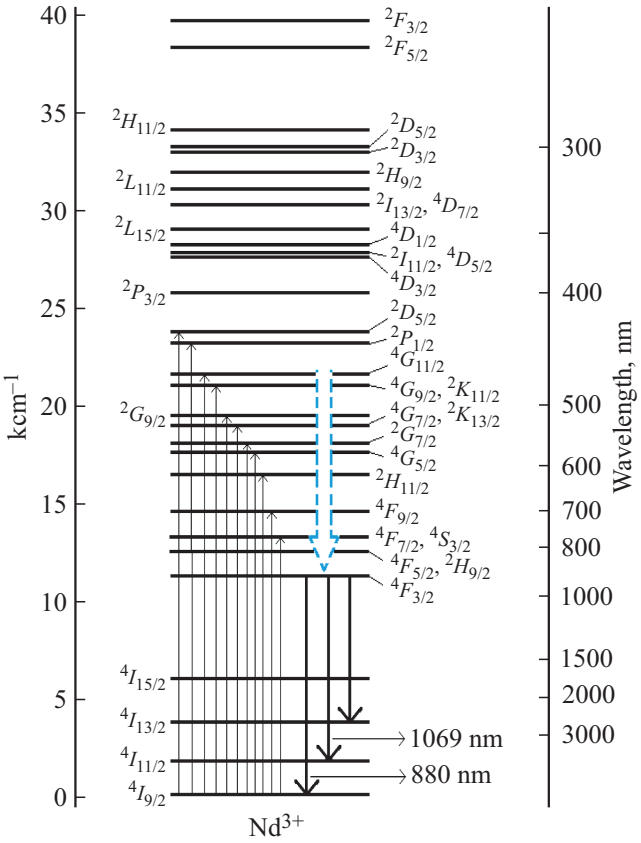

Figure 9. Energy-level diagram for Nd^{3+}.

4. Conclusions

New results on NIR emission in $Na_5Y(WO_4)_4:Nd^{3+}$ are reported. The most intense line is at 1069 nm, which corresponds to $^4F_{3/2} \rightarrow {}^4I_{9/2}$ transition. The excitation and emission spectra can be explained on the basis of the known energy level structure of Nd^{3+}. Though Y−Y distances in this host are as large as 6.39 Å, the concentration quenching is observed for 2 mol.%. The critical distance for energy transfer among Nd^{3+} ions is found to be 32.85 Å. The excitation can be achieved by a large number of $f-f$ transitions spread over entire visible and NIR region, the one at 588 nm being the strongest. A weak host sensitization is indicated by a band at 360 nm in the excitation spectrum.

Acknowledgements

Crystal structure diagrams are prepared using Vesta software. We are grateful to the copyright owners for permitting free use. Assistance in obtaining XRD pattern provided by Shri Shivaji Science College, Amaravati, India is gratefully acknowledged.

Conflicts of interests

The authors declare that they have no conflict of interest.

References

[1] V.K. Trunov, T.A. Berezina, A.A. Evdokimov, V.K. Ishunin, V.G. Krongauz. Russ. J. Inorg. Chem. **23**, 1465 (1978).
[2] P. Ropuszyńska-Robak, L. Macalik, R. Lisiecki, J. Hanuza. Opt. Mater. **110**, 110459 (2020). https://doi.org/10.1016/j.optmat.2020.110459
[3] L.G. Sillén, H. Sundvall, A. Kemi. Mineral. Geol. **17A**, *1*, 1 (1943).
[4] M. Hämmer, O. Janka, J. Bönnighausen, S. Klenner, R. Pöttgen, H.A. Höppe. Dalton Trans. **49**, *24*, 8209 (2020). https://doi.org/10.1039/D0DT00782J
[5] J.I.M. Van Vliet, G. Blasse. J. Solid State Chem. **85**, *1*, 56 (1990). https://doi.org/10.1016/S0022-4596(05)80060-X
[6] D. Qin, W. Tang. RSC Adv. **6**, *51*, 45376 (2016). https://doi.org/10.1039/C6RA10763J
[7] G.N.A. De Guzman, M.-H. Fang, C.-H. Liang, Z. Bao, S.F. Hu, R.S. Liu. J. Lumin. **219**, 116944 (2020). https://doi.org/10.1016/j.jlumin.2019.116944
[8] P. Podemski, A. Marynski, P. Wyborski, A. Bercha, W. Trzeciakowski, G. Sek. J. Lumin. **212**, 300 (2019). https://doi.org/10.1016/j.jlumin.2019.04.058
[9] D. Yang, C. Cao, W. Feng, C. Huang, F. Li. J. Rare Earths **36**, *2*, 113 (2018). https://doi.org/10.1016/j.jre.2017.07.009
[10] G. Blasse. Phys. Lett. A **28**, *6*, 444 (1968). https://doi.org/10.1016/0375-9601(68)90486-6